separations

MDPI

Article

Galvanically Promoted Catalytic Chlorine Activation: Rapid Degradation of Sunset Yellow FCF in a Self-Driven Fe–Cu System

Oualid Hamdaoui *, Abdulrahman Al-Awadi and Abdulaziz Alghyamah

Chemical Engineering Department, College of Engineering, King Saud University, Riyadh 12372, Saudi Arabia
* Correspondence: ohamdaoui@ksu.edu.sa or ohamdaoui@yahoo.fr

Abstract

A self-driven Fe–Cu galvanic couple was investigated for chlorine-mediated degradation of Sunset Yellow FCF (SSY) without external electrical polarization or soluble iron addition. At 20 mg L^{-1} SSY, 600 μM chlorine, initial pH 5, and 25 °C, the normalized SSY signal approached zero within 24 min, whereas electrode-only and chlorine-only controls showed negligible and limited removal, respectively. UV–visible spectral changes supported SSY transformation. Temperature-dependent average rates over 0–3 min yielded an apparent activation energy of 20.4 kJ mol^{-1}. Electrical measurements confirmed galvanic activity, and dissolved total Fe reached 46.6 mg L^{-1} after 30 min in a separate dye-free experiment. However, total organic carbon (TOC) removal was only approximately 12% after 60 min, demonstrating substantial retention of organic carbon despite rapid SSY degradation. The process provides a simple configuration for chlorine-mediated SSY degradation, with iron management and residual organic carbon removal remaining priorities for further development.

Keywords: galvanic coupling; chlorine activation; Sunset Yellow FCF; iron release; water treatment

1. Introduction

Extended molecular conjugation gives azo dyes their intense visible absorption and underpins their usefulness as commercial colorants. Their release into aquatic environments is nevertheless undesirable because even low concentrations can strongly alter water quality and because their extended aromatic structures may resist conventional biological treatment. Sunset Yellow FCF (SSY) is a water-soluble anionic azo dye whose chromophoric system comprises an azo linkage conjugated with aromatic rings and sulfonate groups. This structure produces an intense absorption band in the visible region, typically near 482 nm, together with characteristic bands in the ultraviolet region. Consequently, disappearance of the visible band primarily reflects disruption of the chromophore, whereas concurrent changes in the ultraviolet bands provide additional evidence of transformation of the aromatic structure. Monitoring the complete UV–visible spectrum, rather than color loss alone, is therefore essential for describing SSY degradation. Moreover, total organic carbon (TOC) analysis complements spectrophotometric measurements by distinguishing rapid parent-dye transformation from the subsequent conversion of residual organic carbon [1,2].

Chlorine is an accessible oxidant used extensively in water treatment. In aqueous solution, its reactivity depends on the pH-dependent distribution of hypochlorous acid and

Check for updates

Academic Editors: Milica Petrović, Miloš Kostić, Slobodan Najdanović, Nena Velinov and Miljana Radović Vučić

Received: 23 October 2026
Revised: 6 November 2026
Accepted: 13 November 2026
Published: 16 November 2026

Copyright: © 2026 by the authors. Licensee MDPI, Basel, Switzerland. This article is an open access article distributed under the terms and conditions of the Creative Commons Attribution (CC BY) license.

hypochlorite and on reactions with inorganic and organic constituents [3]. Reactions involving redox-active metals can extend chlorine-mediated oxidation beyond direct chlorination. However, contaminant disappearance alone does not establish detoxification: chlorine-based advanced oxidation can generate transformation products whose toxicological effects require separate assessment [4].

Substrate chemistry also contributes to the pH response. Oakes and Gratton demonstrated pronounced pH-dependent kinetics during hypochlorite oxidation of arylazonaphthol dyes [5]. For SSY, which contains a related conjugated azo–naphthol structure, chlorine speciation must therefore be considered together with substrate reactivity when interpreting changes in treatment performance.

Iron is attractive for chlorine activation because of its abundance, low cost, and redox chemistry. Dissolved Fe(II)/chlorine systems have accelerated the degradation of industrial organic contaminants and textile dyes [6,7]. Liang et al. identified Fe(IV) formation in the Fe(II)/hypochlorous acid reaction [8], while Mao et al. examined contributions from both Fe(IV) and reactive chlorine species during pharmaceutical degradation [9]. More recently, He et al. demonstrated efficient Fe(IV) generation through the Fe(II)/Cl_2 reaction under conditions favoring molecular chlorine [10]. These results show that oxidant assignments depend on the chemical environment rather than following automatically from the presence of iron and chlorine.

Other studies extend this chemistry to defined di-iron complexes reacting with hypochlorite [11], goethite-associated radical chemistry in water-distribution systems [12], and Fe(II)/hypochlorite treatment of fulvic acid [13]. Their distinct iron forms and solution conditions illustrate why observations from one iron/chlorine system cannot identify the dominant pathway in another. They also motivate evaluation of both contaminant transformation and the behavior of iron in a treatment configuration.

Metallic iron offers a practical route for generating dissolved iron in situ, thereby avoiding the direct addition of soluble iron salts. Its performance is governed by interfacial corrosion, solution chemistry, and the formation or dissolution of surface layers [14,15]. When iron is electrically connected to a more noble metal such as copper, a spontaneous galvanic cell is established. Iron functions predominantly as the sacrificial anodic material, while copper provides a cathodic surface for the accompanying reduction reactions. The resulting mixed potential and electron flow can promote iron oxidation and modify the rate at which dissolved iron enters the solution [16]. Because this electrical response arises from the potential difference between the coupled metals, the process requires neither external polarization nor an external electrical power supply. The use of macroscopic Fe and Cu plates also provides a structurally simple and readily separable configuration without requiring the synthesis or dispersion of bimetallic nanoparticles.

Macroscopic Fe–Cu coupling has previously been applied in Galvano-Fenton treatment of Acid Orange 7, combining a spontaneous galvanic cell with peroxide chemistry [17]. Our related steel–copper/peracetic acid (PAA) study demonstrated SSY transformation without soluble iron addition or external electrical polarization [18]. Independent studies have also examined zero-valent Fe–Cu activation of persulfate [19] and Fe(0)/O_2 oxidation enhanced by an air-breathing cathode [20]. These configurations establish the broader relevance of galvanic iron supply, but their oxidants and cathodic reactions differ, requiring system-specific interpretation.

Recent nZVI/chlorine work has demonstrated rapid azo-dye degradation and measurable TOC removal using dispersed nanoscale iron [21]. The present configuration uses electrically connected, readily separable commercial plates. Its evaluation consequently addresses how chlorine-mediated SSY transformation relates to galvanic activity, dissolved-iron accumulation, and organic-carbon removal in a macroscopic treatment system.

This work extends the application of macroscopic Fe–Cu galvanic couples to chlorine-mediated SSY degradation. Its specific contribution is the experimental evaluation of a chlorine-based configuration in which electrically connected commercial plates supply iron in situ, together with assessment of the associated treatment performance and material-release constraints. The configuration operates without external electrical polarization or soluble iron dosing. Controls compare the combined treatment with chlorine alone and connected plates without chlorine, while variations in chlorine dose, initial pH, SSY loading, and temperature establish its operating response.

Complementary electrical measurements and a separate dye-free ICP experiment provide quantitative evidence of galvanic activity and dissolved-iron release. UV–visible spectroscopy and TOC measurements distinguish rapid SSY transformation from organic-carbon removal. Considering these outcomes together identifies both the treatment capability of the Fe–Cu/chlorine configuration and the accompanying iron-management and residual-carbon requirements. Comparison with our related published systems and the independent literature further positions this configuration within the broader field of iron-mediated oxidation.

2. Materials and Methods

Sunset Yellow FCF (SSY; disodium 6-hydroxy-5-[(4-sulfophenyl)azo]-2-naphthalenesulfonate; $C_{16}H_{10}N_2Na_2O_7S_2$; molar mass 452.37 g mol^{-1}; dye content 90%; Sigma-Aldrich, St. Louis, MO, USA) was used as the target compound. A sodium hypochlorite solution (NaClO; approximately 13% active chlorine; CHEM-LAB, Zedelgem, Belgium) was used solely as the source of aqueous chlorine. Dilute sulfuric acid and sodium hydroxide (analytical grade, Sigma-Aldrich) were used for initial-pH adjustment. Solutions were prepared with ultrapure water.

Commercial steel and copper plates were used as the Fe-containing anodic element and the cathodic element, respectively. No soluble iron salt, supporting electrolyte, or external power supply was used. Before each run, the immersed metal surfaces were polished with silicon-carbide abrasive paper up to P4000 grade, rinsed thoroughly with ultrapure water, and dried. Freshly prepared working solutions and cleaned electrode surfaces were used for each independent experimental series.

Experiments were performed in an open glass batch reactor containing 200 mL of solution. The Fe-containing and Cu plates were positioned vertically and parallel to each other, 3 cm apart, with an immersed electrode–solution contact area of 20 cm^2 for each plate. The non-immersed portions and electrical contacts remained above the liquid surface. The plates were connected directly with an insulated wire to form a spontaneous Fe–Cu galvanic couple. The solution was mixed magnetically at a constant speed of 400 rpm and maintained at the selected temperature.

A freshly prepared SSY solution was introduced into the reactor and equilibrated at the selected temperature. The initial pH was adjusted with dilute sulfuric acid or sodium hydroxide, as required, and the solution was left unbuffered. The required volume of freshly diluted chlorine working solution was then added, and immersion of the electrically connected plates defined t = 0. Unless otherwise stated, the reference conditions were 20 mg L^{-1} SSY, 600 µM nominal chlorine, initial pH 5, 25 °C, 400 rpm, and 200 mL. Aliquots were analyzed immediately at the specified treatment times.

SSY was monitored by UV–visible spectrophotometry (Mettler Toledo UV7, Greifensee, Switzerland) in a 1 cm quartz cuvette. The analytical response at 482 nm was converted to apparent SSY concentration using an external calibration relationship. The normalized response was calculated as C/C_0, where C is the apparent SSY concentration at time t and

C_0 is its measured value at t = 0 for the same run. Full spectra from 200 to 600 nm were recorded at 3 min intervals to evaluate changes in both the visible and ultraviolet bands.

Solution pH was measured with a calibrated pH electrode. Galvanic current was recorded by zero-resistance ammetry (ZRA), using a potentiostat equipped with ZRA mode and connected between the Fe-containing and Cu plates in place of the direct wire, and the cell potential was measured across the two electrodes in dedicated electrical measurements. The 30 min and 180 min electrical records were separate experimental runs; current and potential were treated as process diagnostics and were not multiplied to claim a simultaneous power output.

Dissolved Fe release was examined in an independent dye-free experiment containing 600 µM chlorine at initial pH 5 and 25 °C. The aqueous phase was separated from suspended solids before analysis by inductively coupled plasma spectrometry (ICP-OES; ICPE-9820, Shimadzu, Japan). The reported concentration is dissolved total elemental Fe and does not distinguish Fe(II) from Fe(III) or their complexes. TOC was measured with a calibrated total-organic-carbon analyzer (TOC-L, Shimadzu, Japan) and reported as TOC/TOC_0.

3. Results and Discussion

3.1. Process Controls and Spectroscopic Evidence of SSY Degradation

Figure 1 compares the Fe–Cu/chlorine process with chlorine alone and connected Fe–Cu plates without chlorine. The connected plates alone maintained C/C_0 near unity, while chlorine alone produced only a small decline, reaching $C/C_0 \approx 0.91$ after 30 min. Combining chlorine with the connected plates caused the SSY signal to approach zero within approximately 24 min. These results demonstrate enhanced SSY degradation in the combined treatment under the reference conditions.

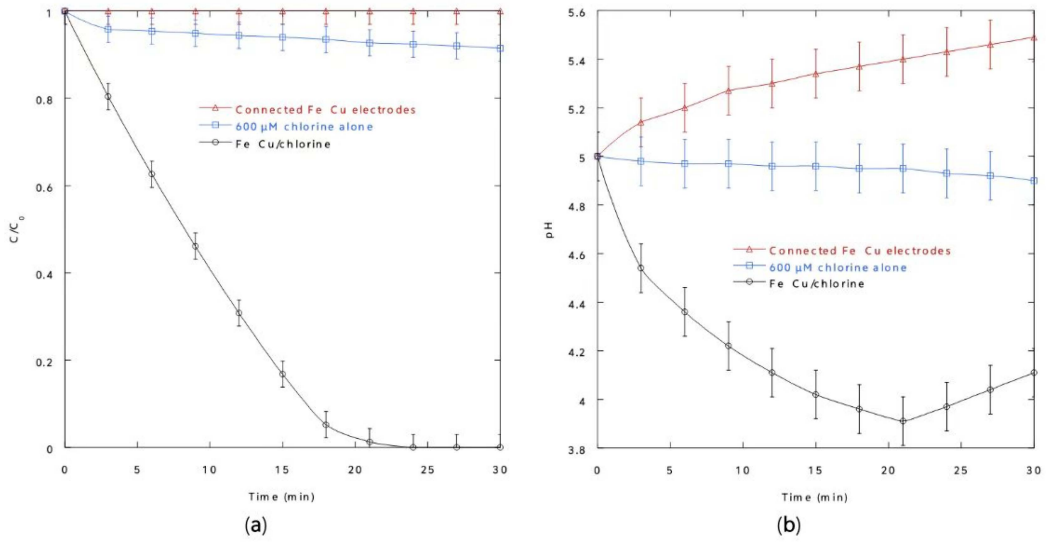


Figure 1. Process controls under the reference conditions: (**a**) normalized SSY response, and (**b**) accompanying pH evolution. Conditions: $[SSY]_0$ = 20 mg L^{-1}, $[chlorine]_0$ = 600 µM, initial pH = 5, T = 25 °C, V = 200 mL, and stirring speed = 400 rpm.

The corresponding pH profiles further distinguish the systems. The electrodes alone caused a modest increase, chlorine alone produced little change, and Fe–Cu/chlorine decreased the pH from 5.0 to approximately 3.9 before a slight recovery. This evolution is compatible with time-dependent iron dissolution, chlorine reactions, and iron hydrolysis, but pH alone cannot separate their contributions [3,15].

Figure 2 provides spectroscopic evidence of SSY transformation beyond the loss of visible color. The initial spectrum exhibited a broad visible maximum near 482 nm and ultraviolet features near 235 and 310–320 nm, consistent with the conjugated dye structure [1,2]. During treatment, the 482 nm band decreased continuously and became indistinguishable from the residual background after approximately 21–24 min. Its disappearance without a pronounced wavelength shift or another visible band supports disruption of the extended chromophoric conjugation.

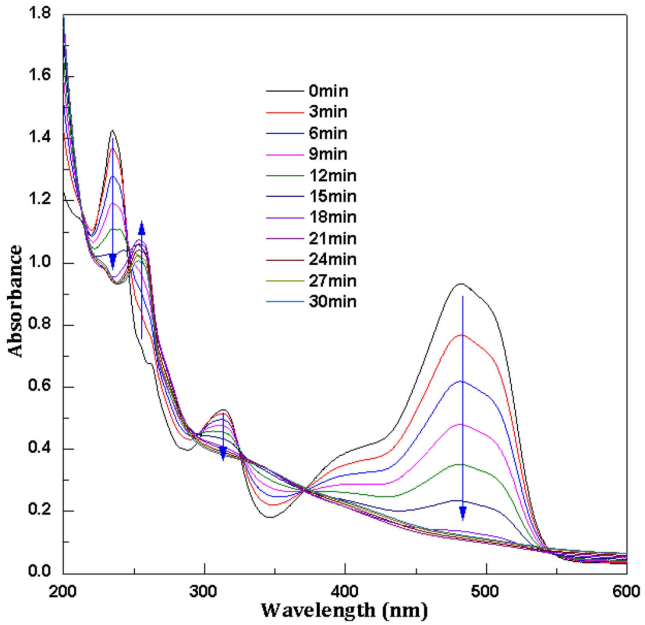


Figure 2. Time-resolved UV–visible spectra during SSY treatment by the Fe–Cu/chlorine process. Conditions: $[SSY]_0$ = 20 mg L^{-1}, $[chlorine]_0$ = 600 µM, initial pH = 5, T = 25 °C, V = 200 mL, and stirring speed = 400 rpm.

The ultraviolet region evolved nonproportionally. As the original bands near 235 and 310–320 nm weakened, the 250–270 nm region became transiently more prominent and the spectral envelope between approximately 330 and 370 nm changed. The crossing of successive spectra is consistent with the formation and transformation of UV-absorbing products. Appreciable ultraviolet absorption remained after disappearance of the visible band, indicating that the spectral endpoint did not correspond to removal of all organic material. These observations support chemical transformation, but do not identify individual products or establish the extent of aromatic-ring cleavage.

The controls and spectra together show that combining chlorine with the metallic plates changes the treatment response beyond that obtained with either component separately. Iron-mediated chlorine activation is a plausible explanation, supported by the independent iron-release measurements in Section 3.6 and by Fe(II)/chlorine studies demonstrating additional oxidative pathways [9]. The present controls do not isolate the individual contributions of steel, copper, and electrical connection; consequently, their specific effects cannot be quantified. The demonstrated outcome is enhanced SSY transformation in the combined treatment, with the fate of organic carbon requiring separate evaluation.

3.2. Chlorine-Dose Threshold and Selection of the Reference Condition

The chlorine-dose series (Figure 3) shows a transition from limited conversion at low dose to a rapid response at higher dose. Doses of 50 and 100 µM were insufficient within 30 min, whereas progressively faster degradation occurred at intermediate doses. At 600 µM

and above, the SSY signal approached zero within approximately 24 min. The convergence of the highest-dose profiles suggests diminishing benefit at the spectral endpoint, although their early kinetics need not be identical.

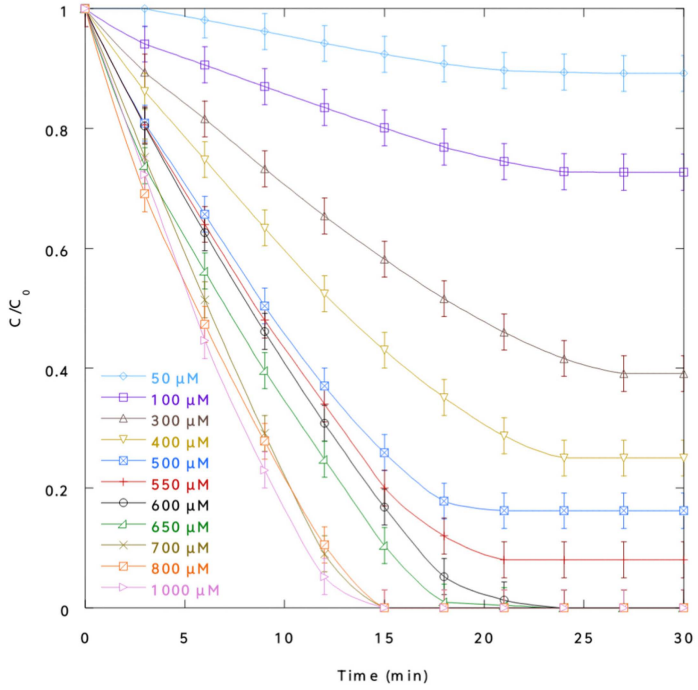


Figure 3. Effect of initial chlorine concentration on normalized SSY degradation by the connected Fe–Cu couple. Conditions: $[SSY]_0$ = 20 mg L^{-1}, initial pH = 5, T = 25 °C, V = 200 mL, and stirring speed = 400 rpm.

A nominal chlorine concentration of 600 µM was selected as the lowest tested dose producing near-complete SSY degradation within approximately 24 min. At 20 mg L^{-1} SSY, this corresponds to a nominal chlorine/SSY molar ratio of approximately 13.6. This ratio is an operating descriptor, not a stoichiometric mineralization requirement. Chlorine participates in both direct substrate reactions and reactions with dissolved iron, so its initial concentration does not directly specify the productive oxidative flux [9,10]. The diminishing improvements at higher doses are consistent with other processes, such as iron supply or reagent transport, becoming increasingly influential. Dose selection should therefore consider both the early response and the required contact time. Because residual chlorine was not measured, 600 µM represents a performance-based reference condition rather than a demonstrated optimum in oxidant utilization.

3.3. pH-Dependent Reaction Windows for Fe–Cu/Chlorine and Chlorine Alone

Figure 4 compares Fe–Cu/chlorine (Figure 4a) with chlorine alone (Figure 4b) over initial pH 1–9. The coupled system reached the spectral endpoint most rapidly at pH 3; pH 4 and pH 8–9 also showed rapid responses, whereas pH 5–7 evolved more slowly. At pH 1–2, early degradation was followed by a pronounced plateau. The overall pH response was therefore non-monotonic.

The paired profiles help distinguish the influence of pH on direct chlorination from the additional effects introduced by the metallic plates. At pH 7–9, rapid degradation also occurred with chlorine alone; at pH 7, its spectral endpoint was reached earlier than in the combined treatment. The plates therefore did not provide uniform enhancement across the investigated pH range. Conversely, the pronounced acceleration at pH 3–6 identifies

conditions under which the plates substantially improved treatment kinetics relative to chlorine alone. The benefit of the combined configuration must consequently be evaluated against the chlorine-only response at the same initial pH.

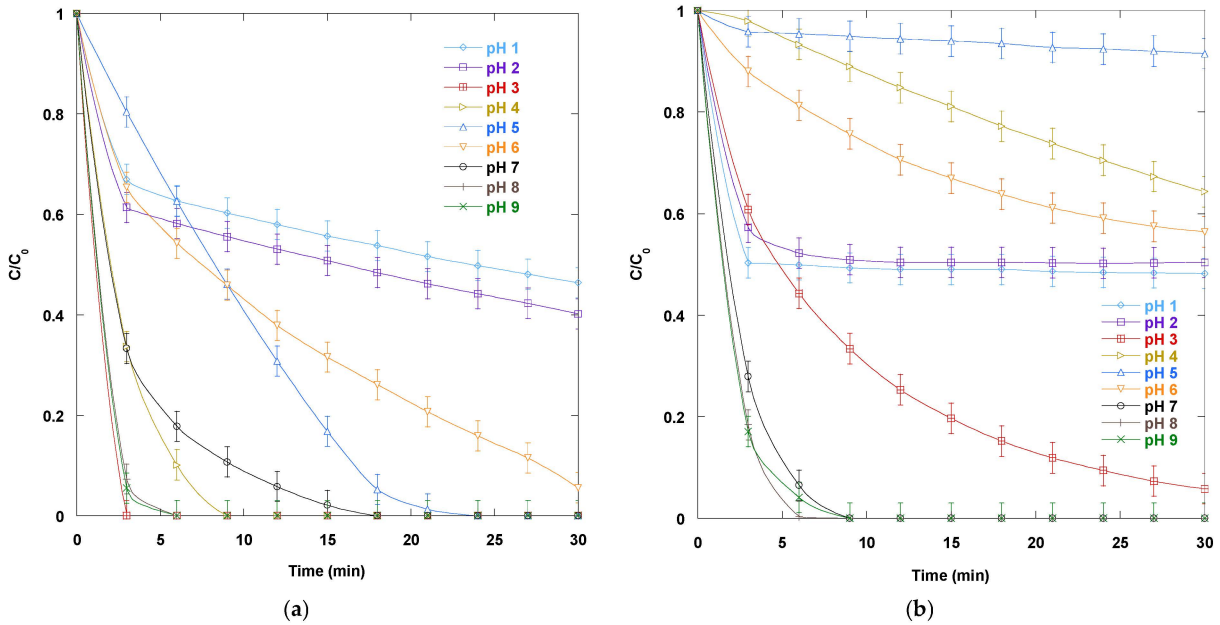


Figure 4. Effect of initial pH on SSY degradation by (**a**) Fe–Cu/chlorine and (**b**) chlorine alone. Conditions: $[SSY]_0 = 20$ mg L^{-1}, $[chlorine]_0 = 600$ µM, T = 25 °C, V = 200 mL, and stirring speed = 400 rpm.

This behavior requires consideration of substrate chemistry as well as chlorine speciation. Experimental studies of related arylazonaphthol dyes show that their susceptibility to chlorine changes with pH [5], while recent Fe(II)/chlorine research demonstrates that solution conditions can alter the reactive pathways [10]. The plateaus at pH 1–2 further show that increasing acidity was not monotonically beneficial. Because the solutions were unbuffered, the reported pH values define starting conditions rather than maintained reaction environments; the profiles consequently cannot identify a unique oxidant or reaction pathway.

3.4. Initial SSY Loading and Finite Oxidative Flux

Increasing the initial SSY concentration progressively slowed fractional degradation at fixed chlorine dose and electrode geometry (Figure 5). The signal approached zero for 3–20 mg L^{-1} within the experimental period, whereas residual C/C_0 values of approximately 0.04 and 0.34 remained at 30 min for 30 and 40 mg L^{-1}, respectively.

The normalized profiles should be interpreted together with the apparent amount of SSY removed. Using the reported 30 min C/C_0 values, initial concentrations of 30 and 40 mg L^{-1} correspond to calculated apparent concentration decreases of approximately 28.8 and 26.4 mg L^{-1}, respectively, compared with approximately 20 mg L^{-1} under the reference condition. Thus, a lower fractional degradation at higher loading can coexist with greater apparent dye removal per unit volume. Nevertheless, the similar magnitudes at 30 and 40 mg L^{-1}, accompanied by poorer fractional conversion at 40 mg L^{-1}, are consistent with a treatment capacity that does not increase proportionally with pollutant loading at fixed chlorine dose and electrode geometry. Competition involving SSY and its transformation products is a plausible contributor. Establishing whether chlorine availability, iron supply, or product reactivity imposes the principal limitation requires additional measurements.

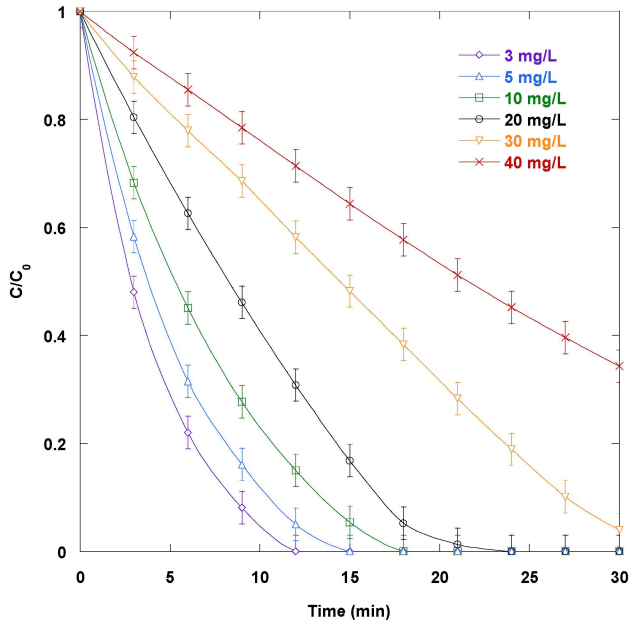


Figure 5. Effect of initial SSY concentration on normalized degradation by Fe–Cu/chlorine. Conditions: $[\text{chlorine}]_0$ = 600 μM, initial pH = 5, T = 25 °C, V = 200 mL, and stirring speed = 400 rpm.

3.5. Temperature Dependence and Apparent Activation Energy

Increasing the temperature from 15 to 45 °C accelerated SSY degradation (Figure 6). No zero-, first-, or second-order rate law was imposed on the curved concentration–time profiles. Instead, the apparent concentration decrease over the same first 3 min was used to calculate an average early-time rate at each temperature:

$$r_{0\text{–}3}(\text{T}) = [\text{C}_0 - \text{C}_3(\text{T})]/(3\ \text{min}) \quad (1)$$

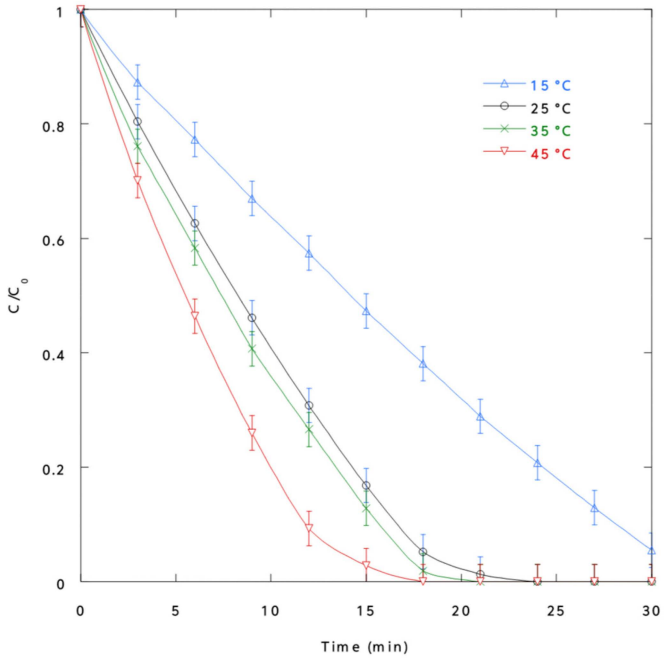


Figure 6. Effect of solution temperature on normalized SSY degradation by Fe–Cu/chlorine. Conditions: $[\text{SSY}]_0$ = 20 mg L^{-1}, $[\text{chlorine}]_0$ = 600 μM, initial pH = 5, V = 200 mL, and stirring speed = 400 rpm.

Here, C_0 and $C_3(T)$ are the apparent SSY concentrations at 0 and 3 min, respectively, and $r_{0–3}(T)$ is expressed in mg L^{-1} min^{-1}. This finite-interval quantity is an average rate rather than the instantaneous initial rate. The initial SSY concentration, chlorine dose, pH, electrode geometry, and mixing conditions were held constant in the temperature series.

The average rates over 0–3 min were 0.87, 1.30, 1.60, and 1.97 mg L^{-1} min^{-1} at 15, 25, 35, and 45 °C, respectively. These rates correspond to approximately 13–30% apparent SSY conversion within the averaging interval, so the interval is not assumed to represent an infinitesimal initial stage. Their temperature dependence was summarized using an Arrhenius-type relationship:

$$\ln[r_{0–3}(T)/r_{ref}] = b - E_{a,app}/(RT) \quad (2)$$

In Equation (2), T is the absolute temperature, and R is the gas constant; the reference rate in the denominator is fixed at 1 mg L^{-1} min^{-1} to make the logarithm dimensionless, and b is an empirical intercept. Regression using the stated rounded rates gives a slope of approximately -2.45×10^3 K and $R^2 \approx 0.978$, yielding $E_{a,app}$ = 20.4 kJ mol^{-1}. The Arrhenius relationship describes temperature dependence and does not establish reaction order, which concerns the concentration dependence of a rate law [22,23]. At a fixed initial composition, a concentration factor in a valid initial-rate law would affect the intercept; it would not determine the reaction order from this plot. Here, the fitted quantity is a finite-interval average rate, so $E_{a,app}$ is an operational descriptor of the overall treatment response, not an activation energy assigned to a validated elementary or global rate constant.

The temperature response integrates iron release, chlorine-mediated reactions, and transport within the coupled system. Increasing the temperature from 25 to 45 °C raised the average early-time rate by approximately 52%, indicating a potential reduction in contact time. Whether heating is advantageous cannot be determined from kinetics alone because the additional energy demand and changes in oxidant utilization were not measured.

3.6. Electrochemical Signatures and In Situ Dissolved-Iron Release

The diagnostics in Figure 7 show galvanic activity over a substantially longer observation period than that required for the SSY spectral endpoint. During the 180 min experiment, current increased to a maximum of approximately 0.73 mA at 27 min and the cell potential rose overall from 179 to 430 mV. The non-monotonic current profile shows that the electrical response evolved during treatment; it does not by itself identify the underlying changes in the electrode interface.

In the extended SSY experiment, the pH reached a minimum of approximately 3.86 at 24 min. The dedicated electrical and pH records indicate evolving reaction conditions, but their timing does not establish a unique sequence of iron dissolution and oxidative conversion. In the independent dye-free experiment, dissolved total Fe rose rapidly and approached 46.6 mg L^{-1} at 30 min, while pH decreased from 5.0 to 3.6. This concentration corresponds to approximately 9.3 mg Fe in 200 mL and should not be interpreted as a simultaneous dissolved-iron measurement during SSY degradation.

ICP quantifies dissolved total elemental Fe; it does not distinguish Fe(II), Fe(III), or their complexes. The measurement therefore establishes iron release without quantifying the concentration of the Fe(II) potentially available for chlorine activation. The resulting aqueous iron concentration also identifies a downstream separation requirement.

Electrical activity and dissolved-iron accumulation describe different aspects of the process. The measured current characterizes electron transfer through the external connection, whereas ICP determines the elemental Fe remaining in the analyzed aqueous phase. A plateau in dissolved Fe therefore does not necessarily indicate that steel corrosion has stopped. It could reflect reduced iron release or a changing balance between release

and transfer into forms removed during phase separation. Such partitioning is chemically plausible given the pH-dependent hydrolysis and solubility of Fe(III) [15], although iron speciation and solid-phase formation were not quantified here. Furthermore, the electrical and dye-free ICP records originated from dedicated experiments, preventing a validated simultaneous electron–iron balance or Faradaic-efficiency calculation. Maximizing current alone is therefore insufficient as an optimization criterion; treatment performance must also be assessed against iron consumption and downstream iron management.

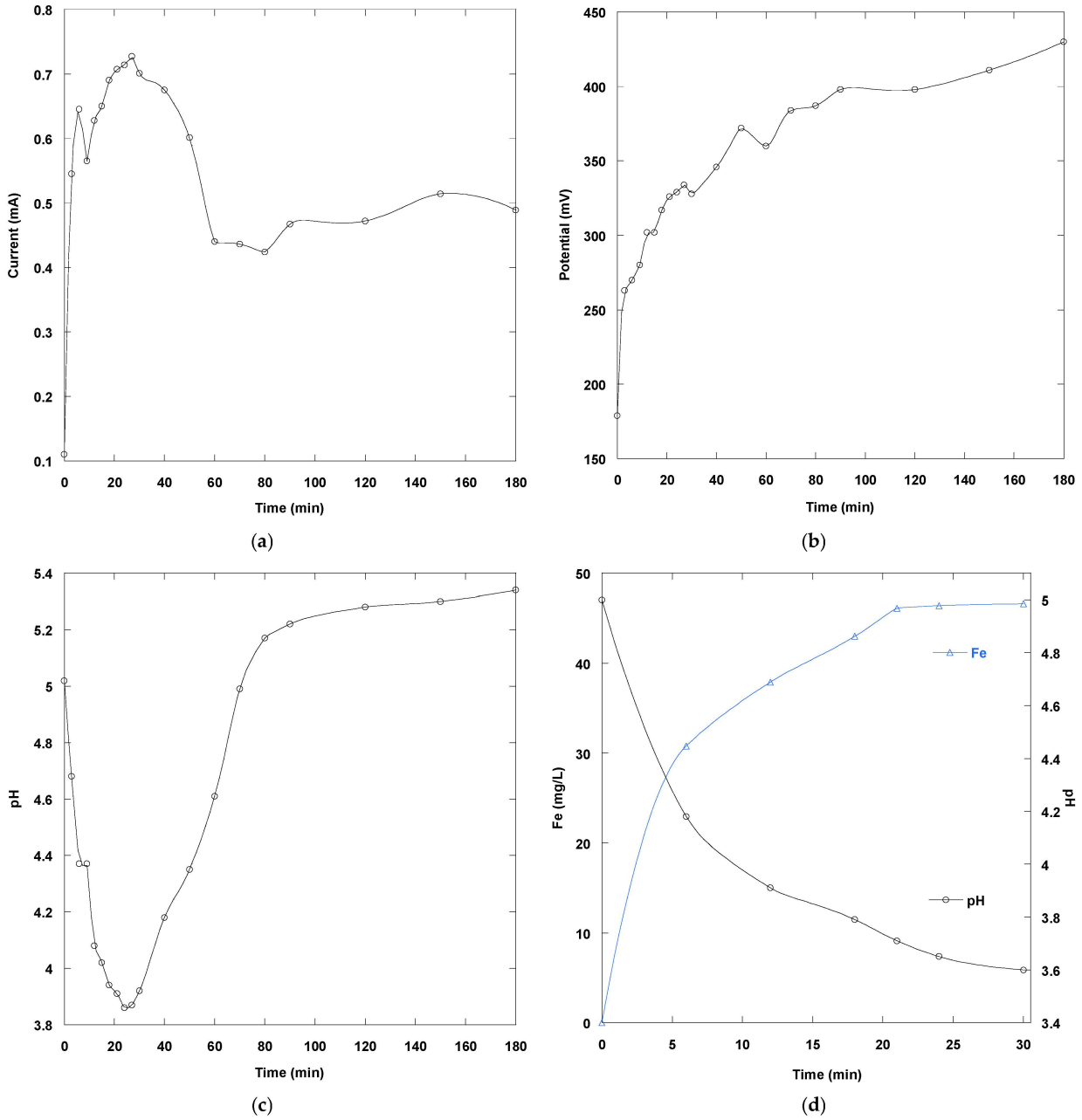


Figure 7. Electrical and iron-release signatures of the Fe–Cu/chlorine process: (**a**) current, (**b**) potential, and (**c**) solution pH over 180 min under the reference SSY condition. (**d**) Dissolved total elemental Fe measured by ICP and accompanying pH in a separate dye-free experiment. Reference condition for (**a**–**c**): $[SSY]_0$ = 20 mg L^{-1}, $[chlorine]_0$ = 600 μM, initial pH = 5, T = 25 °C, V = 200 mL, and stirring speed = 400 rpm. For (**d**), SSY was omitted and all other conditions were unchanged.

3.7. Rapid Spectral Degradation but Persistent Organic Carbon

Figure 8 distinguishes the SSY spectral endpoint from organic-carbon removal. C/C_0 approached zero within approximately 24 min, whereas TOC/TOC_0 was still about 0.88 after 60 min, corresponding to approximately 12% TOC removal. Most of the initial organic carbon therefore remained after transformation of the principal SSY spectral features.

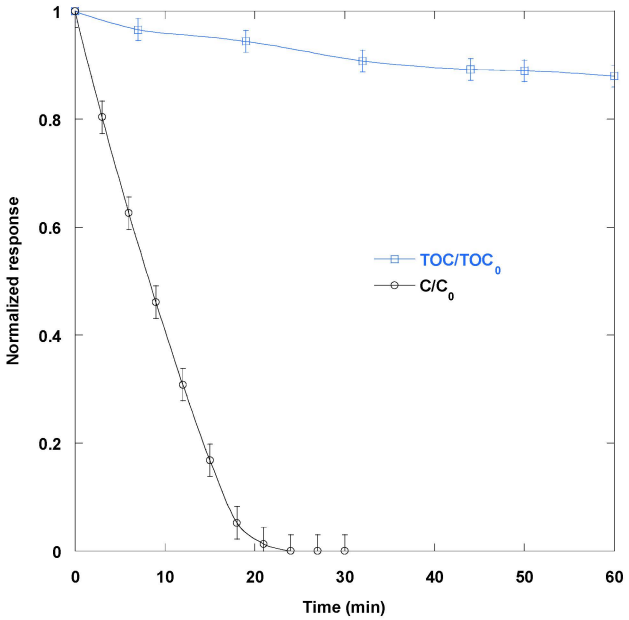


Figure 8. Comparison of normalized SSY response (C/C_0) and normalized total organic carbon (TOC/TOC_0) during Fe–Cu/chlorine treatment. Conditions: $[SSY]_0$ = 20 mg L^{-1}, $[chlorine]_0$ = 600 µM, initial pH = 5, T = 25 °C, V = 200 mL, and stirring speed = 400 rpm.

The separation between the spectral and TOC responses shows that disappearance of the SSY chromophore and removal of organic carbon were distinct treatment endpoints. Changes to conjugation can eliminate the visible dye response while leaving much of its carbon in organic products. The retained TOC is therefore consistent with extensive SSY transformation accompanied by limited carbon removal, although product structures remain unidentified. Together with the extended electrical records, these results also show that continued galvanic activity cannot be assumed to produce equivalent progress in organic-carbon removal. Remaining products may react differently from SSY, while declining oxidant availability could also restrict further conversion; the present measurements cannot distinguish these possibilities. Consequently, treatment duration and reagent dosage should be selected according to the required endpoint, and neither mineralization nor detoxification should be inferred from the SSY spectral endpoint alone.

3.8. Integrated Mechanistic Interpretation and Practical Implications

The principal mechanistic evidence in this study is the combined treatment response. Under the reference conditions, the connected plates without chlorine caused negligible SSY removal, chlorine alone produced a limited response, as shown in Figure 1, and the combined treatment reached the spectral endpoint within approximately 24 min. These observations support a cooperative role of the metallic plates and chlorine. They do not, however, distinguish the separate contributions of steel, copper, and electrical connection because isolated-metal and disconnected-plate controls were not included in this study.

The electrical records establish spontaneous galvanic activity, while the separate dye-free ICP experiment establishes a source of dissolved iron. Together, these observations

support a working interpretation in which corrosion-derived iron contributes to chlorine-mediated transformation. The measured dissolved total Fe does not quantify Fe(II), and the electrical measurements cannot determine how much current leads to productive pollutant oxidation. The activity observed over 180 min also exceeds the time required for the SSY spectral endpoint, showing that continued electrical response and continued organic-carbon removal are separate criteria.

The dose and loading experiments identify a limitation in sustained treatment capacity. At fixed chlorine concentration and electrode geometry, increasing SSY from 20 to 40 mg L^{-1} approximately halves the nominal chlorine/SSY molar ratio, from 13.6 to 6.8, and leaves a residual C/C_0 of approximately 0.34 after 30 min. Additional chlorine above 600 µM gives diminishing improvement at the reference spectral endpoint. These observations favor matching reagent supply and contact time to pollutant loading, rather than treating a larger initial chlorine dose as a proportional increase in productive oxidation. The pH dependence further indicates that this balance changes as solution chemistry evolves.

The carbon measurements set the practical boundary of the demonstrated treatment. Rapid loss of the SSY signal was followed by only approximately 12% TOC removal after 60 min. Thus, the process is effective for SSY transformation under the investigated conditions, while substantial organic carbon remains. The present data do not assign a dominant reactive species or separate homogeneous from surface-mediated oxidation. Published electrochemical iron–oxo and comparative Fe(IV)-oxidation studies provide useful mechanistic context [24,25], but their oxidant assignments cannot be transferred to this reactor without direct evidence.

Table 1 compares the present controls and combined treatment with our related published systems and the independent literature. It identifies the treatment configuration, representative operating conditions, and analytical endpoint so that differences in speed are interpreted with the associated differences in chemistry and pollutant loading.

Table 1. Comparative assessment of the present Fe–Cu/chlorine process and related iron-mediated oxidation systems.

System and Source	Representative Conditions	Reported Outcome and Relevance
Connected Fe–Cu plates; this work	SSY 20 mg L^{-1}; no chlorine; initial pH 5; 25 °C.	C/C_0 remained near unity at 30 min (Figure 1). Metallic plates alone were insufficient.
Chlorine alone; this work	SSY 20 mg L^{-1}; chlorine 600 µM; initial pH 5; 25 °C.	Approximately 9% apparent SSY removal at 30 min in the control (shown in Figure 1).
Connected Fe–Cu/chlorine; this work	SSY 20 mg L^{-1}; chlorine 600 µM; initial pH 5; 25 °C; 200 mL.	C/C_0 approached zero within 24 min; approximately 12% TOC removal at 60 min. Dissolved Fe reached 46.6 mg L^{-1} at 30 min in a separate dye-free run.
Steel–Cu/PAA; Baker et al. [18]	SSY 5 mg L^{-1}; PAA 0.13 mM; natural initial pH ≈ 4.5; 400 rpm.	Approximately 95–96% SSY removal at 5 min; near-complete removal within 7–9 min. Same dye and related plate platform, with a different oxidant and lower dye loading.
Fe(II)/chlorine; Meghlaoui et al. [7]	Textile dyes; Fe(II) 25 µM; initial pH 5.	Strong enhancement of dye removal within 30 s. Soluble Fe(II) was supplied directly; iron availability differs from the plate-fed system.
Fe–Cu/H_2O_2 Galvano-Fenton; Gasmi et al. [17]	Acid Orange 7, 10 mg L^{-1}; pH 3; Fe–Cu galvanic cell.	Dye degradation over 20 min. Related spontaneous iron-supply principle, with peroxide chemistry and a different target dye.
Electro-Fenton; Ghoneim et al. [2]	SSY; pH 3; $FeSO_4$ 0.1 mM; Na_2SO_4 0.05 M; externally polarized electrodes.	Complete visible-color removal reported after 120 min. The study also followed COD and chromatographic changes; those endpoints are distinct from TOC removal.

Table 1. *Cont.*

System and Source	Representative Conditions	Reported Outcome and Relevance
Zero-valent Fe–Cu/persulfate; Fang et al. [19]	2,4-Dichlorophenol; pH 3.3; source-designated Fe/Cu(0.75) catalyst.	Reported rate constant increased from 0.025 min^{-1} for Fe(0) to 0.097 min^{-1} for Fe–Cu. Shows an effect of bimetallic composition within that system.
Fe(0)/O_2 with an air-breathing cathode; Lei et al. [20]	Rhodamine B; galvanic Fe(0) oxidation and passive air supply at the cathode.	Rate constant increased from 0.047 to 1.412 min^{-1} relative to chemical Fe(0)/O_2. Cathodic oxygen supply was an explicit design feature.
nZVI/chlorine; Hamida and Merouani [21]	Model azo dye CG-HG; nZVI 100 mg L^{-1}; chlorine 250 µM.	>95% dye removal within 5 min; 38% TOC removal also reported at its own sampling endpoint. Uses dispersed nanoparticles; TOC and dye-removal times must be distinguished.

PAA: peracetic acid; COD: chemical oxygen demand; nZVI: nanoscale zero-valent iron. Values are representative of the cited studies and are not a ranking under matched conditions. Present-work control values refer specifically to Figure 1. TOC results are reported only where available and at the stated or source-specific sampling endpoint.

The steel–Cu/PAA study is a particularly relevant comparison because it uses SSY and a related macroscopic plate configuration [18]. Its shorter removal time was obtained at 5 mg L^{-1} SSY, one quarter of the present reference loading, and with a different oxidant formulation. The nominal oxidant/SSY molar ratios are approximately 11.8 for PAA and 13.6 for chlorine, but they do not represent equivalent oxidizing capacity or mineralization demand. The commercial PAA formulation also contains hydrogen peroxide. These differences prevent a defensible ranking based on treatment time alone. Likewise, the rapid response of directly dosed Fe(II)/chlorine and the earlier Fe–Cu/H_2O_2 results distinguish iron-delivery and oxidant choices, without establishing that either is intrinsically superior to the present configuration [7,17].

Independent Fe–Cu/persulfate and Fe(0)/air-cathode studies demonstrate improvements relative to their own controls, emphasizing the importance of metal composition and cathodic reactant supply [19,20]. Their fitted rate constants cannot be compared directly with the finite-interval rates reported here because the substrates, oxidants, and kinetic definitions differ. The nZVI/chlorine results also show that rapid dye removal can coexist with incomplete TOC removal [21]. For practical comparison, readily separable plates, soluble-metal dosing, nanoparticle handling, electrical input, and residual iron must therefore be considered alongside a clearly defined spectral, chromatographic, COD, or TOC endpoint.

The resulting development priorities follow directly from the measured performance: determine residual-chlorine utilization, control iron release and separation, and improve removal of the residual organic carbon. Coupling with irradiation is a possible extension supported by UV/chlorine, UV/chlorine/Fe(III), and solar hypochlorite/iron studies [26–28]; any benefit to this configuration remains to be tested against carbon removal, product formation, and irradiation demand.

4. Conclusions

The present work demonstrates chlorine-mediated SSY degradation using a macroscopic Fe–Cu galvanic couple and establishes its operating response through complementary measurements of treatment performance, galvanic activity, dissolved-iron release, and organic-carbon removal. Under the reference conditions, C/C_0 approached zero within 24 min, while the electrode-only and chlorine-only controls in Figure 1 showed negligible and limited removal, respectively. Changes in the visible and ultraviolet spectra supported SSY transformation. A chlorine dose of 600 µM was the lowest tested

condition giving near-complete degradation within approximately 24 min. The fastest combined-treatment response occurred at initial pH 3, while increasing SSY loading reduced fractional conversion at fixed dose and electrode geometry. Average rates over 0–3 min yielded $E_{a,app}$ = 20.4 kJ mol^{-1} without establishing a reaction order or an elementary activation barrier.

Electrical measurements confirmed spontaneous galvanic activity, and dissolved total Fe reached 46.6 mg L^{-1} after 30 min in the separate dye-free experiment, identifying a need for downstream iron management. Although the SSY signal approached zero within 24 min, TOC removal was approximately 12% after 60 min; substantial organic carbon therefore remained. Toxicity was not evaluated, so the observed SSY degradation and TOC removal cannot be interpreted as evidence of detoxification. The comparison with related systems positions the process as a simple configuration for SSY transformation rather than a demonstrated complete-mineralization treatment. Residual-chlorine utilization, transformation-product identification, iron recovery, toxicity assessment, and validation in real waters remain priorities for further development.

Author Contributions: Conceptualization, methodology, formal analysis, writing—original draft preparation, writing—review and editing, supervision, project administration, and funding acquisition, O.H.; investigation, validation, data curation, and visualization, A.A.-A.; validation, visualization, and supervision, A.A. All authors have read and agreed to the published version of the manuscript.

Funding: The authors gratefully acknowledge the financial support provided by the Ongoing Research Funding Program (ORF-2026-2128), King Saud University, Riyadh, Saudi Arabia.

Data Availability Statement: Data are contained within the article.

Conflicts of Interest: The authors declare no conflicts of interest.

References

1. Gosetti, F.; Gianotti, V.; Polati, S.; Gennaro, M.C. HPLC-MS degradation study of E110 Sunset Yellow FCF in a commercial beverage. *J. Chromatogr. A* **2005**, *1090*, 107–115. [CrossRef] [PubMed]
2. Ghoneim, M.M.; El-Desoky, H.S.; Zidan, N.M. Electro-Fenton oxidation of Sunset Yellow FCF azo-dye in aqueous solutions. *Desalination* **2011**, *274*, 22–30. [CrossRef]
3. Deborde, M.; von Gunten, U. Reactions of chlorine with inorganic and organic compounds during water treatment—Kinetics and mechanisms: A critical review. *Water Res.* **2008**, *42*, 13–51. [CrossRef] [PubMed]
4. Sánchez-Montes, I.; Santos, G.O.S.; dos Santos, A.J.; Fernandes, C.H.M.; Souto, R.S.; Chelme-Ayala, P.; El-Din, M.G.; Lanza, M.R.V. Toxicological aspect of water treated by chlorine-based advanced oxidation processes: A review. *Sci. Total Environ.* **2023**, *878*, 163047. [CrossRef] [PubMed]
5. Oakes, J.; Gratton, P. Kinetic investigations of the oxidation of arylazonaphthol dyes in hypochlorite solutions as a function of pH. *J. Chem. Soc. Perkin Trans. 2* **1998**, *27*, 2201–2206. [CrossRef]
6. Behin, J.; Akbari, A.; Mahmoudi, M.; Khajeh, M. Sodium hypochlorite as an alternative to hydrogen peroxide in Fenton process for industrial scale. *Water Res.* **2017**, *121*, 120–128. [CrossRef] [PubMed]
7. Meghlaoui, F.Z.; Merouani, S.; Hamdaoui, O.; Bouhelassa, M.; Ashokkumar, M. Rapid catalytic degradation of refractory textile dyes in Fe(II)/chlorine system at near neutral pH: Radical mechanism involving chlorine radical anion ($Cl_2^{\bullet-}$)-mediated transformation pathways and impact of environmental matrices. *Sep. Purif. Technol.* **2019**, *227*, 115685. [CrossRef]
8. Liang, S.; Zhu, L.; Hua, J.; Duan, W.; Yang, P.-T.; Wang, S.-L.; Wei, C.; Liu, C.; Feng, C. Fe^{2+}/HClO Reaction Produces $Fe^{IV}O^{2+}$: An Enhanced Advanced Oxidation Process. *Environ. Sci. Technol.* **2020**, *54*, 6406–6414. [CrossRef] [PubMed]
9. Mao, Y.; Liang, J.; Ji, F.; Dong, H.; Jiang, L.; Shen, Q.; Zhang, Q. Accelerated degradation of pharmaceuticals by ferrous ion/chlorine process: Roles of Fe(IV) and reactive chlorine species. *Sci. Total Environ.* **2021**, *787*, 147584. [CrossRef] [PubMed]
10. He, S.; Wu, Y.; Qin, W.; Li, S.; Cheng, W.; Li, P.; Wang, S.; Ouyang, G.; Zhu, M.; Fang, J. Efficient generation of highly reactive $Fe^{IV}O^{2+}$ via the Fe(II)/Cl_2 reaction for water purification. *Water Res.* **2026**, *291*, 125219. [CrossRef] [PubMed]
11. McPherson, J.N.; Miller, C.J.; Wegeberg, C.; Chang, Y.; Hedegård, E.D.; Bill, E.; Waite, T.D.; McKenzie, C.J. Cooperative Co-Activation of Water and Hypochlorite by a Non-Heme Diiron(III) Complex. *J. Am. Chem. Soc.* **2021**, *143*, 15400–15412. [CrossRef] [PubMed]

12. Dong, F.; Zhu, J.; Lou, J.; Chen, Z.; He, Z.; Song, S.; Zhu, L.; Crittenden, J.C. Unveiling the Mechanism and Kinetics of Pollutant Attenuation by Free Radicals Triggered from Goethite in Water Distribution Systems. *Environ. Sci. Technol.* **2024**, *58*, 12664–12673. [CrossRef] [PubMed]
13. He, T.; Deng, L.; Lai, B.; Xu, S.; Wang, L.; Zhang, Y.; Zheng, D.; Hu, C. The performance of Fe^{2+}/ClO^{-} system in advanced removal of fulvic acid under mild conditions. *J. Environ. Chem. Eng.* **2022**, *10*, 107515. [CrossRef]
14. Sun, Y.; Li, J.; Huang, T.; Guan, X. The influences of iron characteristics, operating conditions and solution chemistry on contaminants removal by zero-valent iron: A review. *Water Res.* **2016**, *100*, 277–295. [CrossRef] [PubMed]
15. Stefánsson, A. Iron(III) Hydrolysis and Solubility at 25 °C. *Environ. Sci. Technol.* **2007**, *41*, 6117–6123. [CrossRef] [PubMed]
16. Izquierdo, J.; Nagy, L.; Santana, J.J.; Nagy, G.; Souto, R.M. A novel microelectrochemical strategy for the study of corrosion inhibitors employing the scanning vibrating electrode technique and dual potentiometric/amperometric operation in scanning electrochemical microscopy: Application to the study of the cathodic inhibition by benzotriazole of the galvanic corrosion of copper coupled to iron. *Electrochim. Acta* **2011**, *58*, 707–716. [CrossRef]
17. Gasmi, I.; Kerboua, K.; Haddour, N.; Hamdaoui, O.; Alghyamah, A.; Buret, F. The Galvano-Fenton process: Experimental insights and numerical mechanistic investigation applied to the degradation of acid orange 7. *Electrochim. Acta* **2021**, *373*, 137897. [CrossRef]
18. Baker, A.; Hamdaoui, O.; Al-Awadi, A.; El Blidi, L.; Alghyamah, A. Ordinary Steel–Copper Galvanic Cell for Peracetic Acid Activation: A Low-Cost Catalytic Oxidation Process for Sunset Yellow FCF. *Catalysts* **2026**, *16*, 894. [CrossRef]
19. Fang, L.; Liu, K.; Li, F.; Zeng, W.; Hong, Z.; Xu, L.; Shi, Q.; Ma, Y. New insights into stoichiometric efficiency and synergistic mechanism of persulfate activation by zero-valent bimetal (Iron/Copper) for organic pollutant degradation. *J. Hazard. Mater.* **2021**, *403*, 123669. [CrossRef] [PubMed]
20. Lei, Z.; Huang, Z.; Lin, Y.; Liu, Y.; Yan, Z.; Zheng, W.; Ma, H.; Dang, Z.; Feng, C. Boosting the oxidative capacity of the Fe(0)/O_2 system via an air-breathing cathode. *J. Hazard. Mater.* **2022**, *438*, 129552. [CrossRef] [PubMed]
21. Hamida, M.; Merouani, S. Innovative nZVI/chlorine system for efficient micropollutants degradation: Mechanistic insights and process optimization toward sustainable water treatment applications. *Environ. Sci. Water Res. Technol.* **2025**, *11*, 3099–3115. [CrossRef]
22. International Union of Pure and Applied Chemistry (IUPAC). Order of reaction. In *Compendium of Chemical Terminology (the Gold Book)*, 5th ed.; International Union of Pure and Applied Chemistry: Málaga, Spain, 2025. [CrossRef]
23. International Union of Pure and Applied Chemistry (IUPAC). Arrhenius equation. In *Compendium of Chemical Terminology (the Gold Book)*, 5th ed.; International Union of Pure and Applied Chemistry: Málaga, Spain, 2025. [CrossRef]
24. Wang, S.; Wang, C.; Feng, C.; Zheng, W.; Dong, H.; Guan, X. Electrochemically producing high-valent iron–oxo species for phenolics-laden high chloride wastewater pretreatment. *Water Res.* **2024**, *261*, 122068. [CrossRef] [PubMed]
25. Chen, Z.; Wang, Z.; Ma, J.; Li, X.; Zhou, Y.; Gao, Y.; Yang, T.; Zhang, Z.; Wu, Z. Comparative analysis of Fe(IV)-based advanced oxidation processes in generating disinfection byproducts and altering dissolved organic matter molecular structure. *Chem. Eng. J.* **2025**, *512*, 162379. [CrossRef]
26. Fang, J.; Fu, Y.; Shang, C. The Roles of Reactive Species in Micropollutant Degradation in the UV/Free Chlorine System. *Environ. Sci. Technol.* **2014**, *48*, 1859–1868. [CrossRef] [PubMed]
27. Asif, M.; Deng, L.; Mao, Y.; Khan, H.U.; Tang, Q. Efficient degradation of 2-nitrophenol during the UV/chlorine treatment in the presence of Fe(III): Kinetics, DFT calculation and HNMs formation. *J. Environ. Chem. Eng.* **2025**, *13*, 115712. [CrossRef]
28. Pourehie, O.; Saien, J. Solar driven homogeneous sodium hypochlorite/iron process in treatment of petroleum refinery wastewater for reusing. *Sep. Purif. Technol.* **2021**, *274*, 119041. [CrossRef]

Disclaimer/Publisher's Note: The statements, opinions and data contained in all publications are solely those of the individual author(s) and contributor(s) and not of MDPI and/or the editor(s). MDPI and/or the editor(s) disclaim responsibility for any injury to people or property resulting from any ideas, methods, instructions or products referred to in the content.